

Multi-scale Simulation of Solid Oxide Fuel Cell Power Units

Antonio Bertei*, Cristiano Nicolella

Dipartimento di Ingegneria Civile e Industriale, Università di Pisa, Largo L. Lazzarino 2, 56126, Pisa, Italy
antonio.bertei@for.unipi.it

A multi-scale physically-based model is presented in this study in order to quantitatively assess the effect of geometrical modifications and working conditions in an existing SOFC small power unit. The model, validated in different operating conditions, describes transport and reaction phenomena within the electrodes and the feeding channels through conservation equations, while the electrode microstructural properties are evaluated through the particle-based three-dimensional reconstruction of the microstructure. The model is able to capture the main chemical and physical phenomena occurring from the microscale to the macroscale, thus predicting the power output from the knowledge of the same input parameters available in reality, such as powder characteristics and operating conditions. The presented simulations rationalize how the power unit behaves upon a variation in flow configuration, operating temperature and cell geometry, thus providing a tool to predict how to optimize and control the operation of an SOFC system.

1. Introduction

Solid oxide fuel cells (SOFCs) electrochemically convert the chemical energy of a fossil or renewable fuel into electric energy at high temperature (600-1,000 °C) while keeping fuel and oxidizer separated. This feature makes SOFCs one of the most sustainable, clean and efficient technologies to produce electricity for both stationary and mobile applications (Singhal and Kendall, 2003).

An SOFC power unit consists of the assembly of several cells, each of which is made of a dense electrolyte and two electrodes, wherein fuel oxidation and oxygen reduction occur. The electrodes are porous layers consisting of a random dispersion of electron-conducting and ion-conducting particles, mixed together and sintered to promote the transport and reaction processes occurring at the microscale. The complex interplay among the electrode microstructural characteristics (e.g., porosity, composition, particle size), cell geometry (e.g., electrode thicknesses, cell length) and operating conditions (e.g., temperature, fuel and air flow-rates) affects the global rate of conversion of the reactants, thus determining the power density produced by the SOFC unit (Bertei et al., 2012). Hence, it is important to mathematically describe such a complex interplay through a mechanistic model in order to assist the system optimization in design phase and to control the SOFC operation in working conditions.

In this study, a multi-scale physically-based model, based on the numerical reconstruction of the electrode microstructure and the description of transport and reaction processes through conservation equations, is presented and applied to simulate the electrochemical behaviour of an existing SOFC power unit in different operating conditions. The paper is organized as follows. In Section 2 the multi-scale modelling framework is presented. In Section 3 the model is validated and applied to predict the effect of different operating conditions on the power output. The conclusions of the study are reported in Section 4.

2. Multi-scale modelling

Figure 1 shows a schematic representation of a cell of the anode-supported SOFC power unit considered in this study. Fuel gas (i.e., humidified hydrogen) and air are fed by using gas channels and permeate through the electrodes, which are porous composite layers made of electron-conducting and ion-conducting particles. Note that the electrolyte is impermeable to gases since it is a dense ion-conducting layer.

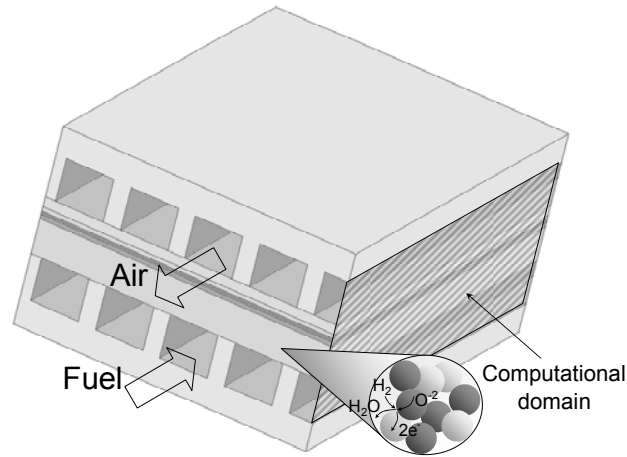


Figure 1: Schematic representation of an anode-supported SOFC

During operation, hydrogen and oxygen are depleted along the channel length due to the electrochemical reactions occurring, respectively, within the anode and the cathode as follows:



Within the electrodes, reactions (1) and (2) occur at the three-phase boundaries (TPB) between gas phase, electron-conducting and ion-conducting particles. As represented in Figure 1, in order to spread the reactions within the whole electrode volume, porous electrodes are fabricated by sintering a random mixture of electron-conducting and ion-conducting particles. In this study, the ion-conducting phase is yttria-stabilized zirconia (YSZ), which is the same material used for the electrolyte, while two different electron-conducting phases are used, which are nickel (Ni) at the anode and strontium-doped lanthanum manganite (LSM) at the cathode. The current production depends not only on the reaction rate at the TPB sites but also on the rate at which gas and charged species are transported within the electrodes. The microstructural characteristics of the electrodes significantly affect the rate of transport and reaction processes, thus affecting the macroscopic performance of the system, such as the power produced by the unit. This complex interplay between microstructural and electrochemical phenomena is taken into account by the multi-scale model: Section 2.1 describes the microstructural model, Section 2.2 the electrochemical model.

2.1 Microstructural modelling

At the microscale, the microstructural model predicts the effective properties of the electrodes (e.g., effective conductivities, tortuosity factors, TPB length per unit volume, etc.) starting from the knowledge of powder characteristics and sintering conditions (i.e., particle size and volume fractions of the conducting phases, porosity, etc.). This is done in two steps: 1) numerical reconstruction of the microstructure of each electrode through a particle-based packing algorithm according to the corresponding powder characteristics and sintering conditions, 2) evaluation of the desired effective properties of the virtual microstructure by means of a random-walk Monte-Carlo algorithm. In this Section, the algorithms adopted for the microstructural characterization of the electrodes are briefly summarized as full details of the microstructural model can be found elsewhere (Bertei et al., 2013a).

The drop-and-roll packing algorithm is adopted in this study in order to numerically generate a three-dimensional virtual sample of the microstructure of each electrode. The algorithm mimics the sequential random deposition of each conducting particle, which drops and rolls over particles already placed until a stable position is reached. The volume fraction and particle size of each conducting phase is enforced during the packing generation. The densification introduced by the sintering process is simulated by allowing particles to overlap during the packing reconstruction. The effect of binders and other organic additives, intentionally introduced in the electrode in order to control the porosity after sintering, is taken into account by dropping particles that vanish after sintering leaving additional pores in the microstructure.

Once the electrode microstructure has been virtually generated, the effective properties of the electrode microstructure are evaluated by a combination of Monte-Carlo techniques and geometrical analysis (Bertei et al., 2013b). The effective diffusivity of the electrode is evaluated by using a random-walk method, which simulates the Brownian motion of thousands of tracers within the pores and determines the effective diffusivity from the mean square displacements through the Einstein equation. The same approach is employed in the solid conducting phases to evaluate the effective electric conductivity. Other properties of the microstructure are determined through a geometrical analysis. In particular, the mean pore size is determined from the corrected number-averaged chord length distribution, while the TPB length per unit volume is evaluated by detecting the contact perimeter between percolating electron-conducting and ion-conducting particles.

2.2 Electrochemical modelling

The electrochemical model describes transport and reaction phenomena within the cell and the gas channels by means of balance equations. At this level (mesoscale), in order to reduce the computational cost without compromising model accuracy, two simplifications are made: 1) the microstructural details are conveniently taken into account by assimilating the electrode microstructure to a homogeneous continuum characterized by effective properties, which are evaluated as described in Section 2.1; 2) only a single repeating unit of the cell is considered, consisting of a two-dimensional slice of the cell as represented in Figure 1.

The set of mass, charge and momentum balance equations is reported in Table 1. Within the electrodes, the right hand side of the molar balance in Eq(3) accounts for the production (or consumption) of the species at the TPB according to the stoichiometry of the electrochemical reactions (Eq(1) or Eq(2)). Note that such a source term is 0 in the electrolyte. The flux of charged species in the electron-conducting and ion-conducting phases is described with the Ohm law (Eq(4)), while the transport of gas species is described with the dusty-gas model (Eq(5)), accounting for both convection, binary and Knudsen diffusion.

The species continuity equation in the gas channels (Eq(6)) takes into account the flux N_i^{cell} that the channel exchanges with the cell due to the electrochemical reactions (1) and (2) occurring within the electrodes. The transport of gas species considers convection, diffusion and axial dispersion (Eq(7)). Finally, Eq(8) represents the momentum balance for a compressible flow in laminar regime. For more details on the electrochemical model, the reader is referred to Bertei et al. (2014).

Table 1: Electrochemical model equations

| Domain | Description | Model equation |
|------------------------------|----------------------|--|
| Electrodes, electrolyte (2D) | Molar balance | $\nabla \cdot N_i = \frac{v_i}{ v_e } \frac{i_{TPB} \lambda_{TPB}}{F}$ (3) |
| | Flux charged species | $N_i = -\frac{\sigma_p^{eff}}{q_i F} \nabla V_p$ (4) |
| | Flux gas species | $\frac{N_i}{D_{i,Kn}^{eff}} + \sum_{j \neq i}^n \frac{y_j N_i - y_i N_j}{D_{i,j}^{eff}} = -\frac{P}{RT} \nabla y_i - \frac{y_i}{RT} \left(1 + \frac{BP}{\mu D_{i,Kn}^{eff}} \right) \nabla P$ (5) |
| Gas channel (1D) | Mass balance | $\frac{d\tilde{N}_i}{dx} = \frac{w+r}{wh} N_i^{cell} M_i$ (6) |
| | Flux gas species | $\tilde{N}_i = \rho v \tilde{y}_i - D_{i,j} \left(1 + Pe^2 \frac{\delta}{210} \right) \rho \frac{d\tilde{y}_i}{dx}$ (7) |
| | Momentum balance | $\frac{d}{dx} \left(\rho v^2 - \frac{4}{3} \mu \frac{dv}{dx} \right) = -\frac{dP}{dx} - 2 \frac{w+h}{wh} \tau_w$ (8) |

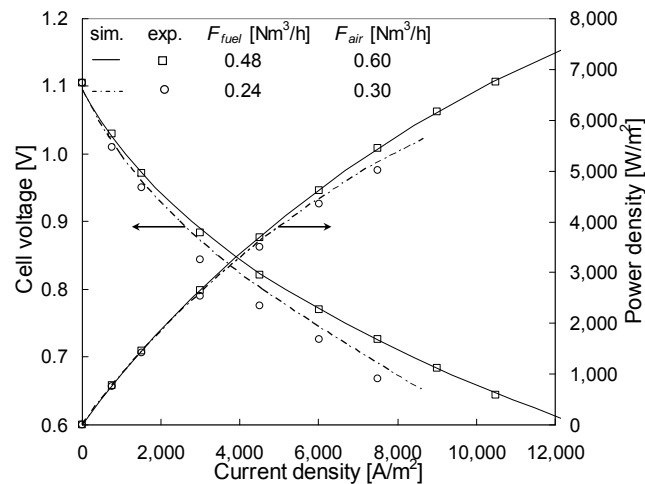


Figure 2: Validation of the multi-scale model against experimental data (Bertoldi et al., 2008) in different operating conditions. Results are referred for a single cell of the SOFC power unit

3. Results

3.1 Validation of the multi-scale model

The multi-scale model described in Section 2 is applied to simulate the macroscopic electrochemical behaviour of an SOFC power unit made of 4 cells 90 mm x 90 mm produced by the Forschungszentrum Jülich. The unit was fed with humidified hydrogen in counter-flow configuration at 800 °C as described by Bertoldi et al. (2008). The geometrical and microstructural characteristics of the cell can be found elsewhere (Bertei et al., 2014).

Figure 2 shows the current-voltage characteristic of the unit for different fuel and air flow-rates. As the current density increases, the cell voltage decreases as a consequence of increased energy dissipations. Notably, less power is produced as both fuel and air flow-rates are reduced. The good agreement between simulation and experimental results confirms the capability of the multi-scale model to predict the macroscopic electrochemical behaviour of the unit starting from powder information and operating conditions. It is noteworthy that no fitted or adjusted parameters were used in the simulation.

3.2 Simulations in different working conditions

The multi-scale model is used in this Section to analyze the macroscopic electrochemical performance of the power unit in different working conditions in order to obtain design indications.

Figure 3a shows the effect of a variation in the air flow-rate. Given the current density, as the air flow-rate increases, the cell voltage increases. This is a consequence of the larger oxygen concentration at the reaction sites in the cathode due to the comparatively lower oxygen depletion along the cell length. The improvement in performance levels off at high air flow-rates, suggesting that once a sufficient oxygen feed is guaranteed, corresponding about to the stoichiometric amount, there is no advantage in further increasing the air flow-rate. The model can be conveniently used to identify the sources of energy losses in the cell as reported in Figure 3a. The Figure shows that the cathode is the main source of energy dissipations, suggesting that further improvements in the cathode are necessary in order to optimize the performance.

The effect of different flow configurations is reported in Figure 3b, which shows the distribution of current density at the anode-electrolyte interface along the cell length. Simulations show that, in both the cases, the local current production is larger at the fuel inlet and then decreases along the cell length because hydrogen is consumed. Notably, at the fuel inlet the local current production is larger in co-flow than in counter-flow configuration due to the larger driving force for the electrochemical reaction in the first case. However, the sharp decrease in current distribution in co-flow configuration leads to a lower mean current density, thus the counter-flow configuration is preferred in order to maximize the power output.

The multi-scale model is used in Figure 4 to predict the current-voltage behaviour for different operating temperatures. Simulation results show that, as the temperature increases, the current density increases at a given cell voltage. This is due to the larger kinetic rates and conductivities, which are both thermally-activated, as the temperature increases.

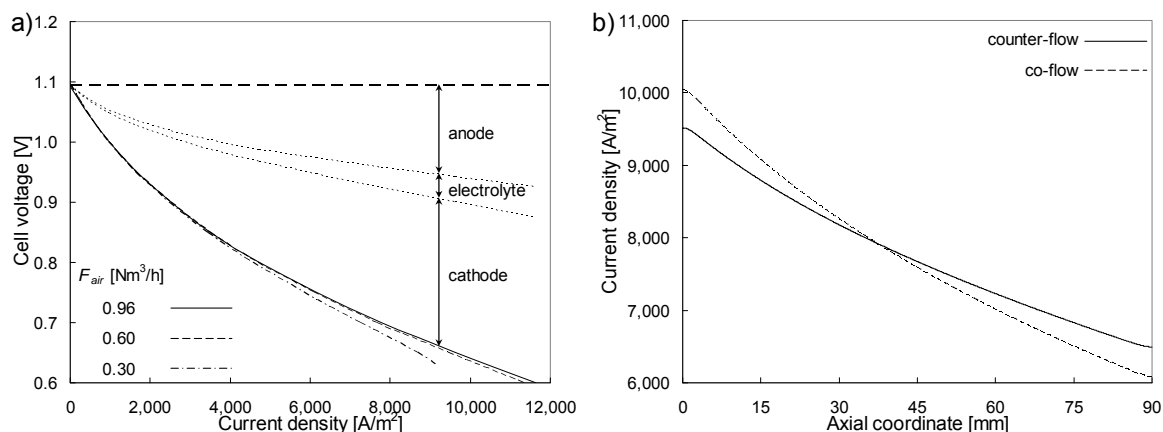


Figure 3: a) Current-voltage characteristic for different air flow-rates; b) Current density distribution along the cell length for counter-flow and co-flow configurations (the fuel inlet is located at $x = 0$)

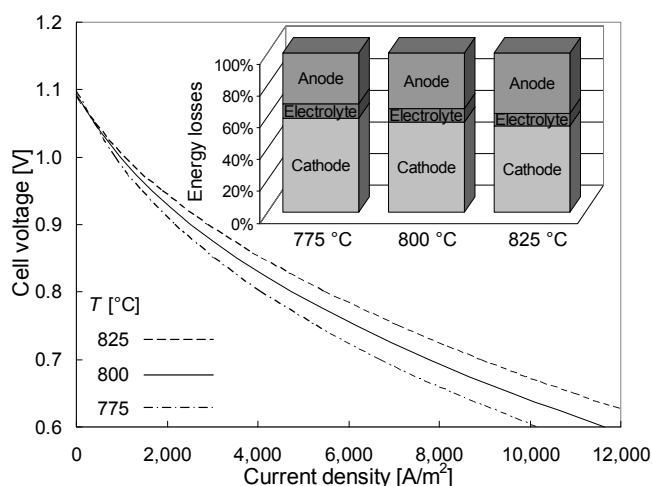


Figure 4: Current-voltage characteristic for different operating temperatures as simulated by the model

Figure 4 also shows the distribution of energy dissipations for different temperatures as predicted by the model. Simulation results show that, as the temperature decreases, the cathode contribution to energy losses increases. This is due to the larger activation energy of the cathodic reaction if compared with the anodic one. A further decrease in temperature would lead to poor power output as a consequence of the reduced catalytic activity of the cathode materials. This result suggests that, in the temperature range 650-750 °C, other conducting materials with larger catalytic activity must be used at the cathode, such as lanthanum strontium cobalt ferrite (LSCF) (Haanappel et al., 2006).

Finally, the model is used to assess the effect of an increase in cell area, from 90 mm x 90 mm to 90 mm x 190 mm, through an increase in cell length while keeping the other conditions unvaried. Note that this modification corresponds to a reduced fuel and air supply per unit of cell area. Figure 5 shows that, as the cell length increases, the current density decreases at a given voltage, corresponding to a reduced power per unit area. This is due to the reduced specific reactant supply per unit area, similarly to what happened in Figure 2. However, given the voltage, the longer cell produces a larger total power output due to the increased cell area: for example, at 0.7 V the longer cell yields 75 W/cell while the shorter cell yields 44 W/cell.

Figure 5 also shows that the longer cell shows a larger electric efficiency. Similarly to heat engines, the electric efficiency is defined as the ratio between the power output and the combustion enthalpy contained in the fuel inlet (Bertei et al., 2014). Because more fuel is consumed in the longer cell and thus more total power output is produced, the electric efficiency increases as the cell area increases given the other conditions. It is noteworthy that even a small SOFC power unit as that analyzed in this study can reach electric efficiencies in the order of 45 % or above as represented in Figure 5.

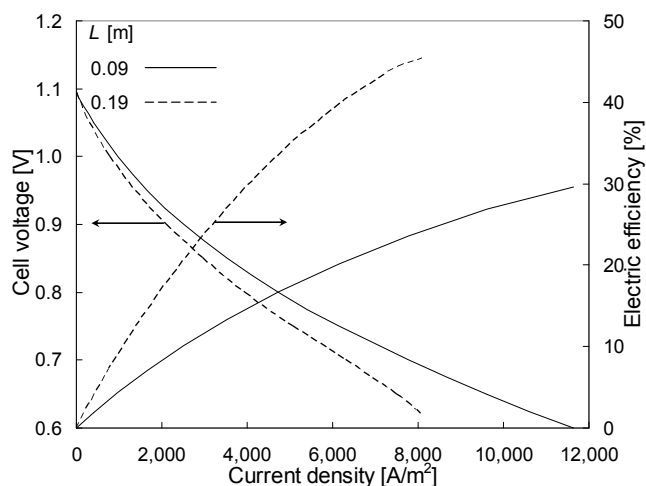


Figure 5: Current-voltage characteristic for different cell lengths as simulated by the model

4. Conclusions

A multi-scale model for the simulation of solid oxide fuel cell power units was presented in this study. The model, based on the microstructural reconstruction of porous electrodes and the mathematical description of transport and reaction phenomena, allowed the physically-based simulation of the system from the microscale to the macroscale with a substantial reduction in unknown parameters. Notably, no fitted or adjusted parameters were necessary for the comparison of model predictions with experimental data.

The model was used to predict the electrochemical behaviour of the power unit in different operating conditions. Simulations showed that the cathode was the main source of energy dissipations and no significant improvement in efficiency was possible by increasing the air flow-rate beyond the stoichiometric requirement. In particular, the cathode contribution to energy losses was found to increase as the temperature decreased, indicating that more catalytic cathode materials must be adopted as the operating temperature is reduced. Finally, model simulations showed that large efficiencies of energy conversion, comparable or even larger than those attained in heat engines, could be obtained by increasing the fuel utilization per unit of cell area.

This study showed that a physically-based multi-scale model can predict quantitative indications without requiring any additional information than those readily available in reality, such as powder characteristics and operating conditions. The presented model is thus a flexible design tool to assist the optimization and to control the performance of solid oxide fuel cell power units.

References

- Bertei A., Barbucci A., Carpanese M.P., Viviani M., Nicoletta C., 2012, Morphological and electrochemical modeling of SOFC composite cathodes with distributed porosity, *Chem. Eng. J.*, 207-208, 167-174.
- Bertei A., Nucci B., Nicoletta C., 2013a, Microstructural modeling for prediction of transport properties and electrochemical performance in SOFC composite electrodes, *Chem. Eng. Sci.*, 101, 175-190.
- Bertei A., Nucci B., Nicoletta C., 2013b, Effective transport properties in random packings of spheres and agglomerates, *Chemical Engineering Transactions*, 32, 1531-1536, DOI: 10.3303/CET1332256.
- Bertei A., Mertens J., Nicoletta C., 2014, Electrochemical simulation of planar solid oxide fuel cells with detailed microstructural modeling, *Electrochim. Acta*, 146, 151-163.
- Bertoldi M., Zandonella T., Haanappel V.A.C., Mertens J., Rimmel J., de Haart L.G.J., 2008, Demonstration of a 4-cells SOFC stack under different experimental conditions, *J. Fuel Cell Sci. Technol.*, 5, 011004.
- Haanappel V.A.C., Mertens J., Mai A., 2006, Performance improvement of (La,Sr)MnO₃ and (La,Sr)_x(Co,Fe)O₃-type anode-supported SOFCs, *J. Fuel Cell Sci. Technol.*, 3, 263-270.
- Singhal S.C., Kendall K., Eds., 2003, *High temperature solid oxide fuel cells: fundamentals, design and applications*. Elsevier, Oxford, United Kingdom.